Materialwiss. Werkstofftech. **2019**, *50*, 646–662 **DOI** 10.1002/mawe.201800175

Laser welding of copper-niobium microcomposite wires for pulsed power applications

Laserstrahlschweißen von Mikro-Verbundwerkstoffen aus Kupfer und Niob zum Einsatz in der Hochspannungsimpulstechnik

N. Višniakov[1], G. Mikalauskas[2], O. Černašėjus[2], J. Škamat[3]

The laser welding of copper-niobium microcomposite wires was investigated. It was determined that the joint structure does not have welding defects, while microscopic examination of the joint cross-section showed that the microstructure of the autogenous weld consists mainly of a copper-based solid solution strengthened by niobium-rich precipitations. The weld obtained with use of filler material consists of two distinct zones, which are formed due to melting of filler wire and microcomposite wire. This structure of the joint provides an insignificant increase in electrical resistance and sufficient ultimate strength and plasticity of the joint. The tensile strength of the sample welded without filler material reaches 335 MPa, but such welded joints are very brittle due to very low ductility. However, an autogenous laser welding joint has about 1.6 times better ductility, and the tensile strength of the joint depends on the applied filler material and is equal to the tensile strength of this material.

Keywords: Copper-niobium microcomposites **/** laser welding **/** welding joint **/** electric cable **/** electrical contact connection

Das Laserstrahlschweißen von Kupfer-Niob-Mikrokompositdrähten wurde untersucht. Es wurde festgestellt, dass die Verbindungsstruktur keine Schweißfehler aufweist, während die mikroskopische Untersuchung des Verbindungsquerschnitts zeigte, dass das Gefüge der autogenen Schweißnaht hauptsächlich aus einer festen Lösung auf Kupferbasis besteht, die durch Niob-reiche Ausscheidungen verstärkt wurde. Die unter Verwendung von Schweißzusatzwerkstoffen erhaltene Schweißnaht besteht aus zwei unterschiedlichen Zonen, die durch Schmelzen von Zusatzdraht und Mikrokompositdraht gebildet werden. Diese Struktur der Verbindung führt zu einer unwesentlichen Erhöhung des elektrischen Widerstands und einer ausreichenden Bruchfestigkeit und Duktilität der Verbindung. Die Zugfestig-

[1] Vilnius Gediminas Technical University, Faculty of Mechanics, Institute of Mechanics, Laboratory of Materials Science, J. Basanavičiaus str. 28, 03224 VILNIUS, REPUBLIC OF LITHUANIA

[2] Vilnius Gediminas Technical University, Faculty of Mechanics, Department of Mechanics and Materials Engineering, J. Basanavičiaus str. 28, 03224 VILNIUS, REPUBLIC OF LITHUANIA

[3] Vilnius Gediminas Technical University, Faculty of Civil Engineering, Institute of Building Materials, Laboratory of Composite Materials, Linkmenų str. 28, 08217 VILNIUS, REPUBLIC OF LITHUANIA

Corresponding author: N. Višniakov, Vilnius Gediminas Technical University, Faculty of Mechanics, Institute of Mechanics, Laboratory of Materials Science, J. Basanavičiaus str. 28, 03224 VILNIUS, REPUBLIC OF LITHUANIA,
E-Mail: nikolaj.visniakov@vgtu.lt

Supporting information for this article is available on the WWW under https://doi.org/10.1002/mawe.201800175

© 2019 WILEY-VCH Verlag GmbH & CO. KGaA, Weinheim

keit der ohne Füllmaterial geschweißten Probe erreicht 335 MPa, jedoch sind solche Schweißverbindungen aufgrund der sehr geringen Duktilität sehr spröde. Eine autogene Laserstrahlschweißverbindung weist eine etwa 1,6-fach bessere Duktilität auf, und die Zugfestigkeit der Verbindung hängt von dem aufgebrachten Füllmaterial ab und ist gleich der Zugfestigkeit dieses Materials.

Schlüsselwörter: Mikroverbundstoffe aus Kupfer und Niob / Laserstrahlschweißen / Schweißfuge / Stromkabel / elektrische Kontaktverbindung

1 Introduction

Magnetic systems are quite simple in their design and use low electrical power, therefore they are popular in various fields of science and industry [1]. The key element of such magnetic systems is the solenoid. The most popular are multilayer wound solenoids. The materials of conductors of such solenoids must be very strong and have good electrical conductivity. Magnetic fields over 45 T can be generated only in the form of short pulses, therefore, the electric cables must stand extreme impact and cyclic heating. For those purposes, composite wires of new types are used: Copper-niobium, copper-silver, copper-based metal matrix composite alloys mixed primarily with aluminium oxide ceramic particles, macrocomposites from a copper wire with stainless steel jackets and others [2-4]. Copper-niobium microcomposite is presently considered as the best-fit of all the above-mentioned types because of the whole set of its unique properties. The strength of a such wire is about 1.5 GPa when the electric conductivity is 67 %–70 % IACS [1]. This material is used in different magnetic installations, but also in levitation transport, high-voltage power lines, induction welding and industrial equipment of thermal treatment. Presently, the construction of solenoids of most magnetic equipment is multisectional, therefore it needs many electric contact connections [5, 6].

In electrical engineering, wire and cable connections may be destructive (screwed) and non-destructive (welded, soldered and pressed). Non-destructive joints are preferable in such a case because microcomposite wires are characterised as of limited capability for deformation. Besides, after magnetic systems enter into operation, access to all connections is very limited. All contact connections must not be the weakest component of the system [7]. However, in practice, only the screwed and soldered conductor connections, which do not demonstrate sufficient reliability and long service life in terms of impact loading and cyclic heating, are used [8]. Therefore, the welded joints are advanced and more reliable. The complexity of selection of welding technologies for those purposes occurs due to the copper-niobium microcomposites structure and production specifics, as well as conditions of exploitation. The structure of copper-niobium microcomposites consists of a copper matrix where very thin niobium threads are integrated [9–11]. The technology of copper-niobium microcomposite production is similar to the process of multistage pressure or diffusion bonding when copper-niobium wire is obtained by multiple plastic deformations of materials. Traditional arc welding methods for connection of microcomposite wires may not be used because of inevitable microcomposite structure melting, overheating of the joined wires and the loss of unique properties. Therefore, one of the most important unsettled problems in the techniques of strong magnetic fields is the creation of a reliable welded connection of microcomposite conductors. This problem theoretically may be solved using special methods of welding.

2 Aim of the investigation

A review of new articles and information concerning patents has shown that this problem is quite new and aspects of the welding of copper-niobium microcomposites have been unstudied or underestimated. The main objective of this investigation, therefore, is to explore the possibility of applying laser welding for the nondestructive connection of copper-niobium conductors and testing the most important properties of laser welding joints.

© 2019 WILEY-VCH Verlag GmbH & CO. KGaA, Weinheim

3 The peculiarities of copper and its alloys' laser welding

The laser beam is one of the highest power density sources suitable for industry. However, unlike the electron beam, a vacuum space is normally not used for laser welding. Laser welding offers many advantages: autogenous welding, welding of high thickness materials, welding of dissimilar materials, hybrid laser welding, remote laser welding, eco-friendly technology, a variety of sources with wavelength from 10.6 μm to 0.532 μm, pulsed and continuous modes [12, 13]. Of the numerous types of laser available today, two still dominate the materials area: carbon dioxide (CO_2) and neodymium-doped yttrium aluminium garnet (Nd:YAG) lasers. Only they can provide a sufficiently high-power beam into the production line. Carbon dioxide lasers usually operate in continuous wave (CW) mode. However, neodymium-doped yttrium aluminium garnet lasers with their capability of operating in high-power continuous wave and pulsed mode and their flexible beam delivery through fibre optics, pose a threat to carbon dioxide. The neodymium-doped yttrium aluminium garnet lasers have the ability of pulse shaping at different pulse repetition rates and pulse durations. This flexibility gives control of the thermal input with precision not previously available in laser welding [14]. For most metal welding applications, the wavelength of the laser is not a significant factor. The exception to this is copper and its alloys. Laser welding of copper is very complicated because copper and its alloys have high thermal conductivity and reflectivity [13]. The absorptivity of different metals depends on the wavelength of the laser radiation. Carbon dioxide lasers typically emit at a wavelength of 10.6 μm. Copper reflects approximately 99 % of the incident light energy of the far infrared wavelength of the carbon dioxide laser. Therefore, copper and its alloys are difficult to weld with carbon dioxide lasers [15]. A neodymium-doped yttrium aluminium garnet laser, which is commonly used for metals welding in the industry, has a wavelength of 1.064 μm. The absorptivity of copper at this wavelength is 2 %–3 % [15]. Thus, 97 %–98 % of the energy of the laser beam is reflected on the copper surface and does not cause heating of the material. Therefore, a special strategy is needed at the beginning of the process. Extremely high power density is required to overcome the reflectivity and heat conductivity. This means that a high laser power (several kW) must be focused on an area of 0.15 mm^2 to 0.05 mm^2 to weld copper of several millimetres in thickness [16].

It is known that a weld can be created either as an individual spot or a seam weld. High power and concertation of energy is needed for copper welding, therefore the continuous wave (CW) lasers are not applicable. Neodymium-doped yttrium aluminium garnet laser works in pulse regime, then a laser can produce a peak power that is greater than its average power [17]. For example, a 400 W pulsed neodymium-doped yttrium aluminium garnet laser can produce peak powers of up to 14 kW for a few milliseconds. Therefore, a pulsed laser is typically used for spot welding, including the spot welding joints of copper. With pulsed lasers, a seam weld is created by a series of overlapping spot welds [13].

The minimum power of neodymium-doped yttrium aluminium garnet laser for copper alloys melting must exceed 300 W [18, 19]. With the commercially available lasers, welds with penetration depths of several millimetres in copper can only be achieved at comparatively low welding speeds ($v < 10\ m{\cdot}min^{-1}$) [20]. At low welding speeds, process instabilities such as weld metal ejections and welding defects usually occur [21]. To weld copper successfully and avoid a blow-out, the process must be started with low laser power, which is linearly increased later. To get a regular and flawless weld seam, the melt pool should be smooth and even near the solidification line. To increase the seam quality, a long and oval melt pool should be established in which the melt turbulences can calm down in the rear part right before solidification. This is hard to accomplish considering how fast copper solidifies. The easiest and most effective parameters to vary are laser power and welding speed because welding depth increases with laser power and decreases with rising welding speed [20, 22].

Weld seams in copper and its alloys are usually softer than the base material. In the presence of hydrogen, oxygen-containing copper may embrittle when heated to temperatures above 1000 K. The copper oxides, which are primarily located at the grain boundaries, are chemically reduced by hydrogen to copper + water, which is connected with an intense volume increase. The resulting steam puts high vapour pressure on the grain boundaries and

© 2019 WILEY-VCH Verlag GmbH & CO. KGaA, Weinheim

generates intercrystalline cracks. Therefore, using a shielding gas (argon 99.998 % purity or gas mixtures) is recommended when copper is welded [16]. Shielding gas with the appropriate composition can influence laser beam absorption by the weld metal surface through affecting plasma and the molten pool surface [23]. Therefore, the weldability of copper has been further improved using techniques that increase the effective absorptivity between material and the laser beam and increase the penetration depth. These techniques include using monatomic argon-diatomic oxygen mixture as an assist gas to promote oxide formation during welding and precoating of the copper workpiece with a metallic (stellite, nickel) or oxide coating before welding [24–27]. Oxidizing or plating the copper surface increases the absorptivity; this permits welding of copper while using much lower laser power [25]. Experimental results show that laser welding efficiency was significantly increased after applying a copper-based nanocomposite absorber. The reflectivity of pure copper was significantly decreased (i. e. ~73 %) after spraying the composite absorber on its surface [28]. Modulation of the output power of neodymium-doped yttrium aluminium garnet laser sources is a reported method of reducing weld metal porosity in copper alloys. The modulation of laser power by a function generator has a mostly positive influence on the laser weld quality in copper [28]. Usually, the laser optics were aligned so that the incident laser beam was 5°–18° to the normal of the sample surface to avoid it from damage by the back reflected light [24, 30, 31].

Copper can be welded by laser beam welding in a vacuum, then weld metal ejections at low welding speeds are prevented. This increase in process stability can be transferred in a high penetration depth at a comparatively low laser power level. Sound welding of copper at a power level between 4 kW and 8 kW (intensity level 50 $kW \cdot mm^{-2}$–80 $kW \cdot mm^{-2}$) of a multimode laser becomes possible without weld metal ejections. A penetration depth of 3 mm is achieved [21]. The dissimilar (e. g. copper with aluminium or steel) butt joints of 1 mm thickness were welded without filler materials using a 350 W pulsed neodymium-doped yttrium aluminium garnet laser and copper-beryllium plate with 0.2 mm nominal thickness [25, 32]. The laser welding wires of diameter from 0.1 mm to 1.0 mm can be used for copper and its alloys laser welding. The application of filler material helps to bridge small gaps and defects; fill non-ideal groove-joint geometries (X or V-shaped joints), influence the chemical composition and properties of the weld; less precise tolerances of the edge preparation and misalignment, beam misalignment [33–35]. Mostly, three types of laser welding wires for copper alloys are available in the market: pure copper (99.9 wt.%–100 wt.%), copper alloy (2.1006 and 2.1461).

Weldability of structural materials as regard laser welding is presented in [12, 36, 37]. In principle, weldability of dissimilar materials is good when the joined materials have a similar range of melting points and melting range. The weldability of materials is poor when the melting point of one material is near the boiling point of another material. The copper and niobium combination is weldable with special precautions because these materials have different melting points. The melting point of copper is 1358 K and its boiling point 2835 K. The melting point of niobium is 2741 K, its boiling point 5200 K. Therefore, alloys having high niobium concentration can be welded by applying conduction mode heating, then copper evaporation is minimal. Conduction mode welding of most parts of metals is performed at low energy density in the range of 10^4 $W \cdot cm^{-2}$–10^5 $W \cdot cm^{-2}$ (typically around 0.5 10^5 $W \cdot cm^{-2}$), forming a weld nugget that is shallow and wide. Transition mode occurs at a medium power density in the range of 10^6 $W \cdot cm^{-2}$, typically around $1 \cdot 10^6$ $W \cdot cm^{-2}$, and it results in a deeper penetration than conduction mode. Increasing the peak power density beyond $1.5 \cdot 10^6$ $W \cdot cm^{-2}$ shifts the weld to keyhole mode, which is characterized by deep narrow welds with an aspect ratio greater than 1.5. A critical energy density of about $2.6 \cdot 10^6$ $W \cdot cm^{-2}$ is required for laser melting of copper [36, 38, 39]. A critical power density $3 \cdot 10^6$ $W \cdot cm^{-2}$ and pulse energy 40 J is sufficient to start melting copper with a focused laser beam (spot size about 0.05 cm) [31]. Keyhole initiation in a 1 mm thick pure copper plate was observed at a power density of $5.9 \cdot 10^6$ $W \cdot cm^{-2}$ and pulse energy of 10.5 J.

Therefore, in principle, the welding of copper-niobium conductors must be done with power density larger than $3 \cdot 10^6$ $W \cdot cm^{-2}$ and less than $5.9 \cdot 10^6$ $W \cdot cm^{-2}$. Much higher power density is very harmful for welding because the material is in-

© 2019 WILEY-VCH Verlag GmbH & CO. KGaA, Weinheim

Table 1. Chemical composition and mechanical properties of laser welding wires.

Tabelle 1. Chemische Zusammensetzung und mechanische Eigenschaften von Laserstrahlschweißdrähten.

Material of wire	Composition [wt.%] Copper	Iron	Manganese	Silicon	Zinc	Tin	Nickel
2.0091 (Cu)	99.9	<0.005			<0.0004	<0.002	
2.1006 (CuSn1)	98.0		<0.25	<0.4		0.8	<0.3
2.1461 (CuSi3Mn1)	95.73	0.07	1.0	3.0	0.1	0.1	

tensively evaporated and splashed, the fluid phase practically is not present in the laser action area.

In this work we present the experimental results of copper-niobium wire joining applying the neodymium-doped yttrium aluminium garnet laser welding technology. The present research is aimed at investigating the structure, electric and mechanical properties of laser welding joints of copper-niobium conductors, usable for pulsed magnetic systems.

Table 2. Properties of laser welding wires for copper alloys laser welding [41].

Tabelle 2. Eigenschaften von Laserstrahlschweißdrähten für Kupferlegierungen beim Laserstrahlschweißen [41].

Properties	Material of wire 2.0091 (Cu)	2.1006 (CuSn1)	2.1461 (Cu-Si3Mn1)
Hardness HBW [kgf mm^{-2}]	≤ 50	60	80
Yield strength *Re* [MPa]	55	75	120
Tensile strength *Rm* [MPa]	<255	220	350
Elongation *A* [%]	25	30	40
Thermal conductivity *K* [W m^{-1} K^{-1}] at room temperature	401	145	35
Electrical conductivityIACS [%]	100	72	7
Melting point [K]	1358	1293–1323	1183–1298

4 Materials and welding equipment

The commercially available microcomposite wire copper-niobium (82 wt.%–18 wt.%) with 1.7 mm × 0.8 mm cross-sectional area was used for this research. The wire was manufactured using the 'assembly-deformation' method. The mechanical properties of this wire are as follows: yield strength *Re* is 830 MPa–850 MPa, ultimate tensile strength *Rm*-1120 MPa, elongation after fracture *A*-4.2 % [40]. The Ø 0.3 mm laser welding wire (2.1006) was used for microcomposite conductors laser welding with filler material, *Table 1*. This filler material has better mechanical strength than pure copper wire due to the combined effect of all the alloying elements that are in the mixture, *Table 2*. The electrical conductivity of this filler material is equal to copper-niobium microcomposite wire, which is very important for electrical connections. The melting point of copper-tin alloy (2.1006) is similar to the copper matrix of copper-niobium microcomposite. Therefore, the filler metal will melt when it is added to the weld pool and create a more homogeneous weld after the crystallization stage.

The laser welding machine (BMM400 CNC, China) with 4D positioning table, digital observation system (CCD) and programming software (CNC2000) were used for samples' welding. The 400 W laser power of this laser machine is sufficient for fine details from copper alloys' welding, *Table 3*.

5 The methodology of calculation of laser welding regimes

The critical power density for material melting and evaporation by a laser in the pulse mode can be calculated according to the following Equation 1 or Equation 2 [19, 42–44]:

© 2019 WILEY-VCH Verlag GmbH & CO. KGaA, Weinheim

Table 3. Characteristics of BMM CNC laser welding machine.

Tabelle 3. Eigenschaften der Laserstrahlschweißmaschine CNC BMM 400.

Technical parameters	Range
Laser working substance	Nd:YAG
Maximum single-pulse energy [J]	150
Maximum peak power [kW]	14
Laser wavelength [nm]	1064
Spot size (diameter) [cm]	0.01–0.3
Average laser power [W]	400
Pulse duration [ms]	0.5–10
Pulse frequency [Hz]	0–20

$$P_d = \frac{k(T_e - T_0)\sqrt{\pi}}{2A\sqrt{a\,t_p}} \quad (1)$$

or

$$P_d = \frac{\rho(T_e - T_0)ch}{A\,t_p} \quad (2)$$

where P_d is the critical power density [W·m^{-2}]; A is the absorptivity $A = (1\text{-}R)$; R is the reflection coefficient; k is the thermal conductivity [W·m^{-1}·K^{-1}]; c is the specific heat [J·kg^{-1}·K^{-1}]; a is the thermal diffusivity, [m^2·s^{-1}]; T_o is the initial (room) temperature [K]; T_e is the heating temperature (material melting or evaporation temperature) [K]; ρ is the density [kg·m^{-3}]; t_p is the duration of laser pulse [s]; h is the thickness of the material [m].

The physical properties of joined material for calculations was taken from the literature, *Table 4*. Knowing the critical amount of energy needed to heat the material to the required temperature (melting or evaporation), it is also possible to predict the required critical power of laser radiation by Equation 3 [46]:

$$P_p = P_d S \quad (3)$$

where S is the the spot area [m^2]; P_d is the critical power density [W·m^{-2}]; P_p is the critical peak power [W].

The spot area is described by Equation 4 [44]:

$$\mathrm{S} = \frac{1}{4}\pi d^2 \quad (4)$$

where d is the spot diameter [m].

The peak power density is dependent on pulse energy and beam diameter [14, 46]:

$$P_d = \frac{P_p}{S} = \frac{4\,P_p}{\pi d^2} = \frac{4\,E_p}{\pi d^2 t_p} \quad (5)$$

where d is the spot size [m]; S is the spot area [m^2]; E_p is the pulse energy [J]; t_p is the pulse duration [s]; P_p is the peak power [W].

The relation between single-pulse energy, average laser power and pulse frequency are described by Equation 6 [14, 47]:

$$E_p = \frac{P_m}{f} \quad (6)$$

where E_p is the single-pulse energy [J]; P_m is the average laser power [W]; f is the pulse frequency [Hz].

The maximum peak power is an important parameter, which is required to overcome the reflectivity and heat conductivity of welded materials. The maximum peak power can be obtained according to Equation 7 [14, 47]:

Table 4. Physical properties of copper-based material [45].

Tabelle 4. Physikalische Eigenschaften des Materials auf Kupferbasis [45].

Evaporation temperature T_e [K]	Melting temperature T_m [K]	Absorptivity A	Reflection coefficient R	Thermal conductivity K [W m^{-1} K^{-1}] at room temperature	Thermal diffusivity a [m^2 s^{-1}] at room temperature
2835	1358	0.02	0.98	401	0.12 10^{-3}

© 2019 WILEY-VCH Verlag GmbH & CO. KGaA, Weinheim

$$P_p = \frac{E_p}{t_p} \tag{7}$$

where P_p is the peak power [W]; E_p is the single-pulse energy [J]; t_p is the pulse duration [s].

The average laser power can be obtained according to Equation 8 [14]:

$$P_m = E_p f = \frac{E_p}{t_p}\frac{t_p}{t_f} = P_p C_d \tag{8}$$

where E_p is the single-pulse energy [J]; f is the pulse frequency [Hz]; t_p is the pulse duration [s]; t_f is the the pulse-to-pulse time [s]; C_d is the duty cycle.

The pulse frequency during the pulse welding with the neodymium-doped yttrium aluminium garnet laser is determined by the welding speed. The pulse frequency, spot diameter and welding speed must be consistent among themselves when it is needed to achieve hermetic and sound welds.

The optimal welding speed can be determined according to Equation 9 [13]:

$$v = d\,(1 - P_{er}/100)f \tag{9}$$

where v is the welding speed [mm·s^{-1}]; d is the laser spot diameter [mm]; P_{er} is the spot overlap coefficient [%]; f is the pulse frequency [Hz].

The typical overlapping coefficient for laser welding joints is in the range 70 %–80 %. Increasing overlap percentage provides a penetration closer to the maximum penetration. The dependence between pulse frequency, spot diameter, welding speed and overlap coefficient is presented in Equation 10 [48]:

$$P_{er} = 100\frac{d - {}^{v}/_{f}}{d} \tag{10}$$

where P_{er} is the spot overlap coefficient [%]; d is the laser spot diameter [mm]; v is the welding speed [mm·s^{-1}]; f is the pulse frequency [Hz].

At this time, there are many different laser welding weld depth accessible calculation methods, some of which are in reviewed sources [15, 47]. The width of weld or depth of penetration can be approximately determined according to Equation 11 [44]:

$$Z = \sqrt{at_p} \tag{11}$$

where Z is the width of weld or deep of penetration [m]; a is the thermal diffusivity [m^2·s^{-1}]; t_p is the duration of the laser pulse [s].

6 Calculation and selection of welding parameters

Knowing the physical properties of copper and the typical pulse duration (1 ms–20 ms) for most of the industrial neodymium-doped yttrium aluminium garnet lasers, the critical energy density for laser pulse welding of copper-niobium microcomposites can be calculated by Equation 1. The critical energy density P_d value should be greater than 3 10^6 W·cm^{-2} and close to 5.9 10^6 W·cm^{-2}. Such conditions are best suited for welding modes with a pulse duration of 5 ms–7 ms, then the energy density will be from 4.93 10^6 W·m^{-2} to 5.84 10^6 W·m^{-2}, *Table 5*. Modes with a very short pulse duration of 1 ms–4 ms and greater than 7 ms are not suitable. In the first case, the high energy levels produce metal evaporation and spattering, and in the second case, in contrast, the energy level will not be enough to melt the metal or create the optimal shape weld. The minimum diameter of the laser spot on the surface of the sample in most industrial neodymium-doped yttrium aluminium garnet lasers is about 0.01 cm, the maximum with which copper was thoroughly dissolved −0.06 cm.

Table 5. Range of critical power density P_d [W cm^{-2}].

Tabelle 5. Bereich der kritischen Leistungsdichte P_d [W cm^{-2}].

Pulse duration t_p [ms]	Critical peak power density P_d [W cm^{-2}]
1	13.06 10^6
2	9.23 10^6
3	7.54 10^6
4	6.53 10^6
5	5.84 10^6
6	5.33 10^6
7	4.93 10^6
8	4.62 10^6
9	4.35 10^6
10	4.13 10^6

© 2019 WILEY-VCH Verlag GmbH & CO. KGaA, Weinheim

The laser beam power P_p, depending on pulse duration and laser beam diameter, is calculated according to Equation 3. Laser radiation power P_p, which is required for welding (when using a 0.01 cm–0.06 cm diameter spot and 1 ms–7 ms impulses) ranges from 387 W (0.4 kW) to 36829 W (36.8 kW), *Tables 6, 7*. In the case of a laser beam of 0.055 cm–0.06 cm in diameter and 5 ms–7 ms impulses, the laser radiation power P_p varies from 11684 W (11.7 kW) to 16468 W (16.5 kW). With a 400 W neodymium-doped yttrium aluminium garnet pulsed laser welding, it is possible to achieve a power P_p output of 14 kW, Table 3. Welding modes that require an output of more than 14 kW are not possible with this welding equipment. According to that, welding of copper-niobium conductors must be done with power density larger than $3{\cdot}10^6$ W·cm^{-2} and less than $5.9{\cdot}10^6$ W·cm^{-2} and pulse energy has to be not less than 40 J, the three welding modes can be selected.

Table 6. Range of peak power P_p [W].

Tabelle 6. Bereich der Spitzenleistung P_p [W].

Spot size d [cm]	Spot area S [m^2]	Pulse duration t_p 1 [ms]. Critical peak power density P_d 13.06 10^6 [W cm^{-2}]	Pulse duration t_p 2 [ms].Critical peak power density P_d 9.23 10^6 [W cm^{-2}]	Pulse duration t_p 3 [ms].Critical peak power density P_d 7.54 10^6 [W cm^{-2}]	Pulse duration t_p 4 [ms].Critical peak power density P_d 6.53 10^6 [W cm^{-2}]	Pulse duration t_p 5 [ms]. Critical peak power density P_d 5.84 10^6 [W cm^{-2}]	Pulse duration t_p 6 [ms]. Critical peak power density P_d 5.33 10^6 [W cm^{-2}]	Pulse duration t_p 7 [ms]. Critical peak power density P_d 4.93 10^6 [W cm^{-2}]
0.01	7.85 10^{-5}	1025	724	592	512	458	418	387
0.015	1.76 10^{-4}	2298	1624	1327	1149	1027	938	867
0.02	3.14 10^{-4}	4101	2898	2368	2050	1833	1674	1548
0.025	4.90 10^{-4}	6399	4523	3694	3199	2862	2612	2416
0.03	7.06 10^{-4}	9220	6516	5323	4610	4123	3763	3481
0.035	9.61 10^{-4}	12550	8870	7246	6275	5132	5122	4738
0.04	1.25 10^{-3}	16325	11537	9425	8162	7300	6662	6162
0.045	1.59 10^{-3}	20765	14676	11988	10382	9286	8475	7838
0.05	1.96 10^{-3}	25597	18091	14778	12798	11446	10447	9663
0.055	2.37 10^{-3}	30952	21875	17869	15476	13841	12632	11684
0.06	2.82 10^{-3}	36829	26028	21262	18414	16468	15031	13902
0.065	3.31 10^{-3}	43228	30551	24957	21614	19330	17642	16318
0.07	3.84 10^{-3}	50150	35443	28953	25075	22426	20467	18931
0.075	4.41 10^{-3}	57594	40704	33251	28797	25754	23505	21741
0.08	5.02 10^{-3}	65561	46335	37851	32780	29317	26757	24748

© 2019 WILEY-VCH Verlag GmbH & CO. KGaA, Weinheim

Table 7. Relation between pulse duration, peak power and pulse energy.

Tabelle 7. Beziehung zwischen Impulsdauer, Spitzenleistung und Impulsenergie.

Pulse duration t_p 1 [ms]		Pulse duration t_p 2 [ms]		Pulse duration t_p 3 [ms]		Pulse duration t_p 4 [ms]		Pulse duration t_p 5 [ms]		Pulse duration t_p 6 [ms]		Pulse duration t_p 7 [ms]	
Peak power P_p [W]	Pulse energy E_p [J]	Peak power P_p [W]	Pulse energy E_p [J]	Peak power P_p [W]	Pulse energy E_p [J]	Peak power P_p [W]	Pulse energy E_p [J]	Peak power P_p [W]	Pulse energy E_p [J]	Peak power P_p [W]	Pulse energy E_p [J]	Peak power P_p [W]	Pulse energy E_p [J]
1025	1.0	724	1.5	592	1.8	512	2.1	458	2.3	418	2.5	387	2.7
2298	2.3	1624	3.2	1327	4.0	1149	4.6	1027	5.1	938	5.6	867	6.0
4101	4.1	2898	5.8	2368	7.1	2050	8.2	1833	9.2	1674	10.0	1548	10.8
6399	6.4	4523	9.0	3694	11.1	3199	12.8	2862	14.3	2612	15.7	2416	16.9
9220	9.2	6516	13.0	5323	16.0	4610	18.4	4123	20.6	3763	22.6	3481	24.4
12550	12.5	8870	17.7	7246	21.7	6275	25.1	5132	25.6	5122	30.7	4738	33.2
16325	16.3	11537	23.1	9425	28.3	8162	32.6	7300	36.5	6662	40.0	6162	43.1
20765	20.7	14676	29.3	11988	35.9	10382	41.5	9286	46.3	8475	50.8	7838	54.9
25597	25.6	18091	36.2	14778	44.3	12798	51.2	11446	57.2	10447	62.7	9663	67.6
30952	30.9	21875	43.7	17869	53.6	15476	61.9	13841	69.2	12632	75.8	11684	81.8
36829	36.8	26028	52.1	21262	63.8	18414	73.6	16468	82.3	15031	90.2	13902	97.3
43228	43.2	30551	61.1	24957	74.9	21614	86.5	19330	96.6	17642	105.8	16318	114.2
50150	50.1	35443	70.9	28953	86.8	25075	100.3	22426	112.1	20467	122.8	18931	132.5
57594	57.6	40704	81.4	33251	99.7	28797	115.2	25754	128.8	23505	141.0	21741	152.2
65561	65.5	46335	92.7	37851	113.5	32780	131.1	29317	146.5	26757	160.5	24748	173.2

© 2019 WILEY-VCH Verlag GmbH & CO. KGaA, Weinheim

It is known that the three laser welding parameters significantly affect the penetration depth. To achieve maximum penetration, the laser power has to be a maximum focused on the surface ($F = 0$) while welding speed has to be minimum. The welding speed and focus position are the most important factors affecting the welded zone and heat-affected zone (HAZ) width. An increase in welding speed leads to a decrease in weld and heat-affected zone width. A wide defocused laser beam and an increase of laser power slightly increase the weld width. As the focus position goes into the metal ($F < 0$) the penetration depth significantly reduces and the heat-affected zone width slightly reduces, but weld width increases [49].

Depending on the characteristics of the laser welding equipment used, welding modes Nr. 5–7 can be considered as optimal in this case, *Table 8*. The depth of penetration of copper-niobium wire joints welded applying the Nr. 5–7 welding regimes according to equation 11 must be approximately in the range of 0.8 mm–0.9 mm. Therefore, single-side and both-sides welding can be used for the joining of 0.8 mm thickness copper-niobium microcomposite wire. In practice, the both-sides welded joints are preferable from a strength point of view.

7 Welding procedures and methodology of joints testing

The following welding parameters were used for butt welding of samples from both sides: single-pulse energy 69 J, peak power 14 kW, pulse width 5 ms, pulse frequency 6 Hz, laser spot size Ø 0.055 cm, welding speed 38 mm·min^{-1}, part-to-part gap ~0.2 mm.

The welding was done without filler material (autogenous) and using copper-tin (2.1006) laser welding wire of Ø 0.3·mm diameter. A 45° angle between the beam and the wire for welding with filler material was used.

The samples were clamped in a standard welding fixture. The fixture was mounted on a 3D stage, which provided motion of the workpiece relative to a stationary laser beam. Monatomic argon −3 % diatomic oxygen (M13-ArO-3) gas mixture was used as the shielding gas during all the experiments. The gas was supplied at a flow rate of 10 l/min through a copper pipe of 10 mm internal diameter. During all experimental trials, the laser beam was inclined at 5° from the normal to the sample surface, to minimise back reflections.

For the measurements of electrical resistance, three fragments of copper-niobium wire with butt joints were prepared. Each sample was 30 cm long. The experiments were done according to the methodology explained in the standards [50, 51]. The electrical resistance was measured using a U2810D Digital LCR Meter Tester (China). The Joule heat-

Table 8. Range of optimal welding parameters.

Tabelle 8. Bereich der optimalen Schweißparameter.

Welding regime	Pulse energy E_p [J]	Pulse frequency f [Hz]	Peak power P_p [W]	Spot diameter d [cm]	Pulse duration t_p [ms]	Critical power density P_d [W cm^{-2}]	Welding speed V [mm/min]
1	12.5	32	12550	0.035	1	$13.06 \cdot 10^6$	134
2	23.1	17.3	11537	0.04	2	$9.23 \cdot 10^6$	83
3	35.9	11.1	11988	0.045	3	$7.54 \cdot 10^6$	60
4	51.2	7.8	12798	0.05	4	$6.53 \cdot 10^6$	47
5	69.2	5.8	13841	0.055	5	$5.84 \cdot 10^6$	38
6	75.8	5.3	12632	0.055	6	$5.33 \cdot 10^6$	35
7	97.3	4.1	13902	0.06	7	$4.93\ 10^6$	29
8	104.2	3.8	13028	0.06	8	$4.62\ 10^6$	27
9	110.4	3.6	12267	0.06	9	$4.35\ 10^6$	26
10	136.7	2.9	13670	0.065	10	$4.13\ 10^6$	23

© 2019 WILEY-VCH Verlag GmbH & CO. KGaA, Weinheim

ing of the samples was observed with a Flir-E49001 (Japan) thermal imaging camera. The samples were heated electrically with 60 A using a welding rectifier VDU-305 (USSR). The temperature distribution at the beginning of the experiment and after every 30 seconds was registered.

The face of the welds was inspected visually by a 10× loupe and by higher magnification optical microscopy, to determine the imperfections (spatter, porosity). GE ERESCO 42MF4 (US) radiographic device, scanner Duerr NDT CR 35 NDT (Germany), digital imaging software D-test viewer 9.3 were used for non-destructive testing. The mechanical properties of the welded joints were determined via a tensile test. Three welded butt joints, each 30 cm in length, were tested. The universal tensile press TIRAtest 2300 (Germany) with the Katman-Express software, dynamometer up to 20 kN were used. The selected welds were cross-sectioned to assess the weld profile. The microstructure of the joint was analysed using scanning electron microscopy (SEM) and optical microscopy. For the microscopic investigation, the samples were prepared by abrasive grinding and diamond polishing and subsequently etched using a solution of 8 g copper (II) chloride and 100 ml ammonia (25 %). A scanning electron microscope JEOL JSM-7600 (Japan) equipped with an energy dispersive spectrometer (EDS) Oxford INCA Energy X-Max20 (UK) for chemical microanalysis and optical microscope Nikon MA-200 (Japan) with a digital camera were used.

8 Experimental results and discussion

The laser butt welds without and with filler material are welded, *Figures 1, 2*. The general criteria for the quality of the welds are weld geometry, mechanical properties of the joint, quantity and size of internal and surface defects, chemical composition and weld microstructure. The quality of the obtained joints was evaluated through radiographic non-destructive testing. No unacceptable internal welding defects (cracks, porosity, inclusions, other discontinuities) were observed from the digital X-ray images.

The microstructure and form of laser welds can be observed from the cross-section of joints, *Figures 3*, *4*. In both cases (with and without filler material) weld joints without lack of fusion and penetration or other discontinuity at the interface were formed by laser welding. The edges of the copper-niobium wire can be clearly identified from the view; however, the edges were melted completely and the solid transition without any discontinuities was formed.

The main parameters defining the dimensions of the cross-section of the laser welding joint are the weld thickness or depth of penetration h and width of weld w. As can be seen from the cross-section view of the laser weld, the copper-niobium con-

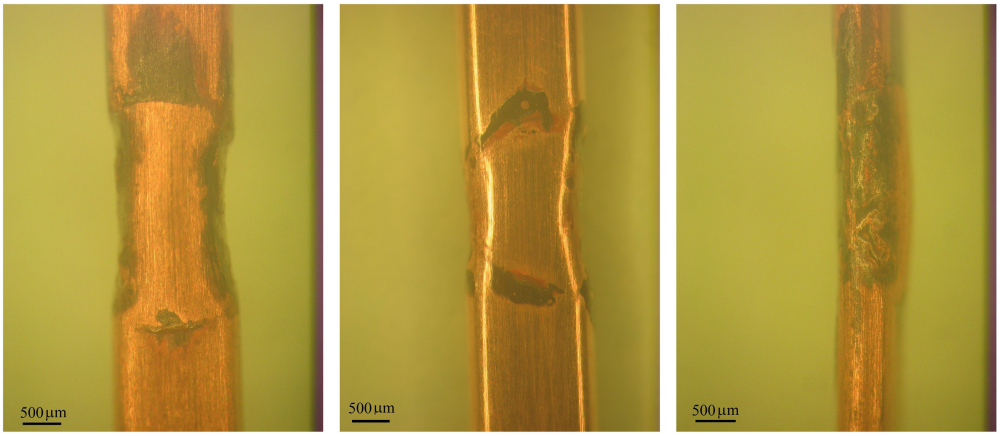


Figure 1. General view of copper-niobium wire butt joint after post-weld mechanical cleaning (autogenous welding): a) Top view of joint; b) bottom view of joint; c) front view of joint.

Bild 1. Allgemeine Ansicht der Kupfer-Niobium-Drahtstoßfuge nach der mechanischen Reinigung nach dem Schweißen (autogenes Schweißen): a) Ansicht der Fuge von oben; b) Ansicht der Fuge von unten; c) Vorderansicht des Gelenks.

© 2019 WILEY-VCH Verlag GmbH & CO. KGaA, Weinheim

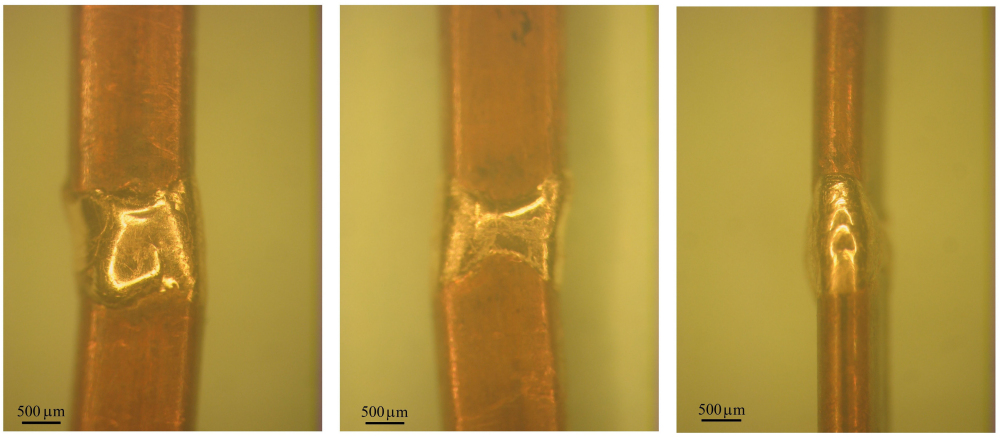


Figure 2. General view of copper-niobium wire butt joint (welding with filler material): a) Top view of joint; b) bottom view of joint; c) front view of joint.

Bild 2. Allgemeine Ansicht der Kupfer-Niobium-Drahtstoßfuge (Schweißen mit Füllmaterial): a) Ansicht der Fuge von oben; b) Ansicht der Fuge von unten; c) Vorderansicht des Gelenks.

ductor wire edges were melted, Figures 3, 4. The maximum penetration or melt pool depth is equal to conductor thickness. The width of weld after welding without filler wire is ~3.0 mm, width of weld after welding with filler wire is ~1.8 mm. The width of the seams welded with filler material is narrower and the dimensions of the weld pool are smaller because under the same welding conditions part of the energy is used to melt the filler wire. The welds with shape coefficient $\psi = \frac{h}{w} \leq 0.5 - 0.7$ are preferable from a strength point of view [58]. The shape coefficient of copper-niobium conductor welding joints in this case is 0.26-0.44, which passes the requirements.

In the weld obtained with filler material, two distinct zones with different composition and microstructure can be seen, Figure 3b, d. The middle part of the weld (zone 2) consists mainly of copper (~84 wt.%) and niobium (~15 wt.%) in a proportion close to the chemical composition of the initial copper-niobium wire, indicating that here the weld was formed mainly due to the melting of the copper-niobium conductor, *Table 9*. As can be seen from elemental maps for copper and niobium, the microstructure of weld zone 2 is composed of fine near-uniaxial niobium particles in the copper matrix, Figure 3e, f. Because copper and niobium have a negligibly low mutual solubility in the solid state, the copper-rich and niobium-rich terminal solid solutions-based mechanical mixture is typical for the microstructure

Table 9. Chemical compositions (by energy-dispersive X-ray spectroscopy analysis) of regions 1 and 2, Figure 3b.

Tabelle 9. Chemische Zusammensetzungen (durch energiedispersive Röntgenspektroskopieanalyse) der Bereiche 1 und 2, Bild 3b.

Region	Chemical elements [wt%]			
	Copper	Niobium	Tin	Other
1	96.94	0.96	0.61	1.49
2	83.66	14.23	–	2.11

of copper-niobium alloys. The size of niobium globules is very small (as compared with copper-niobium microstructure after conventional processing) – from tenth or hundredth of micrometre up to few micrometres. This may contribute to the strength of the weld. The outer part of the weld (zone 1) consists of ~97 wt.% copper, indicating that here the weld was formed mainly due to the melting of filler wire, Figure 3b. The amount of other elements is ~3 %, *Table 10*. In the case of autogenous welding, the weld showed more uniform microstructure and composition across the whole cross-section, *Figure 4*a–d. The elemental composition of weld metal insignificantly differs from the initial copper-niobium wire, Table 10. Its microstructure consists mostly of two phases: copper-rich and niobium-rich terminal solid solutions. A laser-welding procedure promotes the

© 2019 WILEY-VCH Verlag GmbH & CO. KGaA, Weinheim

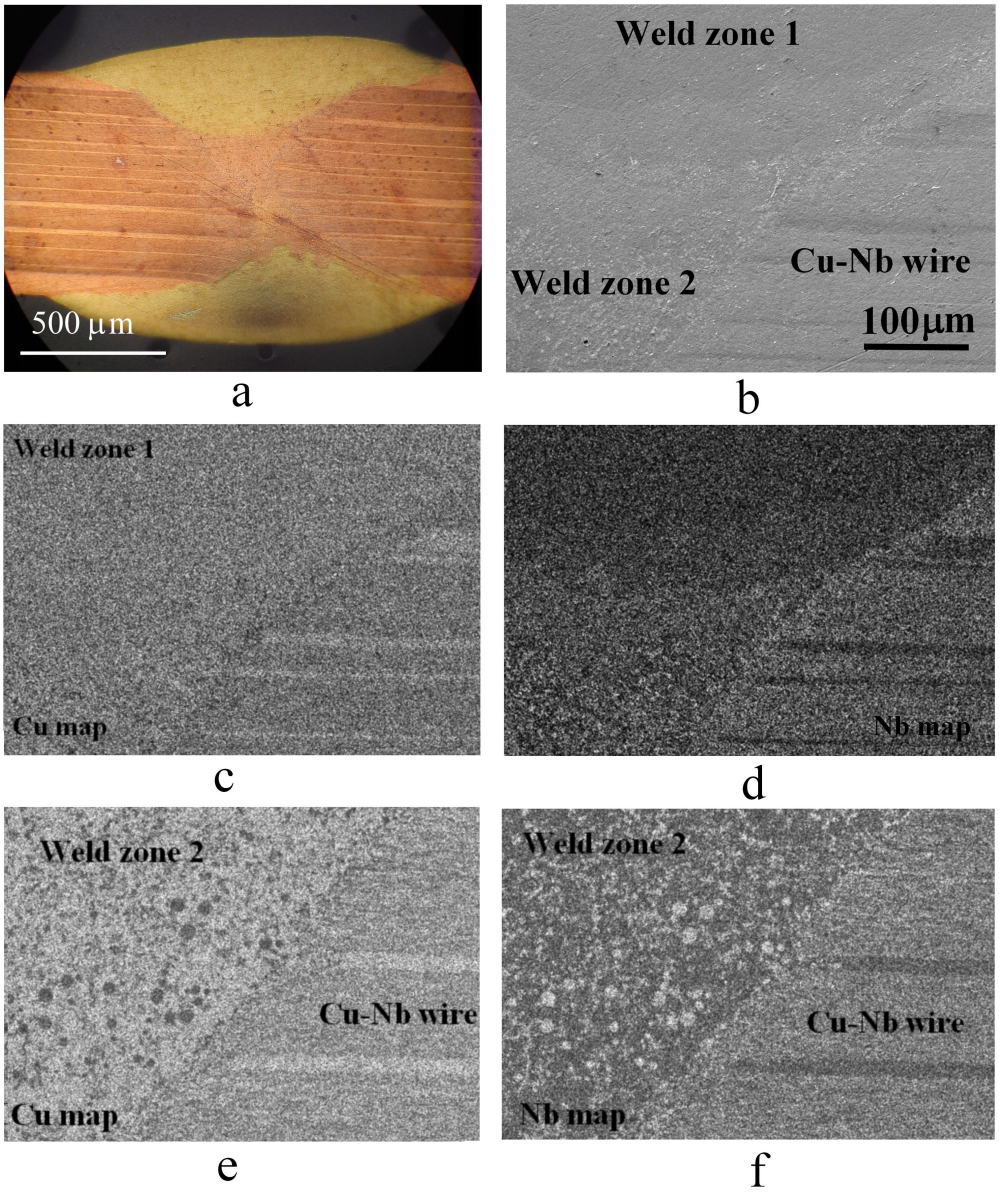


Figure 3. The structure of a joint welded with filler material: a) Longitudinal section of joint; b) Enlarged scanning electron microscope image of microstructure near the interface between the conductor and the weld; c) element map of copper in a weld area Nr. 1; d) element map of niobium in a weld area Nr. 1; e) element map of copper in a weld area Nr. 2; f) element map of niobium in a weld area Nr. 2.

Bild 3. Struktur einer mit Füllmaterial verschweißten Fuge: a) Längsschnitt der Fuge; b) vergrößertes Rasterelektronenmikroskopbild der Mikrostruktur nahe der Grenzfläche zwischen dem Leiter und der Schweißnaht; c) Elementkarte von Kupfer in einem Schweißbereich 1; d) Elementkarte von Niobium in einem Schweißbereich 1; e) Elementkarte von Kupfer in einem Schweißbereich 2; f) Elementkarte von Niobium in einem Schweißbereich 2.

uniform distribution of the niobium in the copper matrix, Figure 4c, d.

To estimate the mechanical and electrical properties of the obtained joints, several tests were carried out. The electrical properties of the samples with a welded joint and the conductor without joint were compared by measuring the difference in their electrical resistances. The conductor of 30 cm length had an electrical resistance of 0.01 Ω at room temperature. The slight increase in resistance was obtained in conductors with a laser welding joints. The samples with welded joints of the same length had an electrical resistance of 0.011 Ω. The difference in electrical resistance was not significant (1.1

© 2019 WILEY-VCH Verlag GmbH & CO. KGaA, Weinheim

Table 10. Chemical compositions (by energy-dispersive X-ray spectroscopy analysis) of regions 1 and 2, Figure 4b.

Tabelle 10. Chemische Zusammensetzungen (durch energiedispersive Röntgenspektroskopieanalyse) der Bereiche 1 und 2, Bild 4b.

Region	Chemical elements [wt%]		
	Copper	Niobium	Other
1	86.71	10.79	2.50
2	79.03	18.41	2.56

times) and it did not exceed the standards recommended limit. The maximum difference in electrical resistance between conductor and samples with welding joint can't reach 1.5 times [51].

Heating of the samples with the welded joint when electrical current flows was registered using a thermal imaging camera. The temperature differences in the laser welding joints and conductor when electrical current flowed did not exceed the recommended value of 95 K [51], *Figure 5*.

The tensile testing of samples with welded joints shows that all specimens break through the weld area. The connection welded with filler material withstood the tensile loads of about 340 N, *Figure 6*. Accordingly, the tensile stress in the area of the fracture reached 250 MPa, which is adequate to 22.3 % of the tensile strength of the initial microcomposite wire, Figure 6. The percentage elongation of the sample of such connection after fracture was 2.5 %. This is about 59.5 % of the microcomposite wire percentage elongation. The connection welded without filler material withstood the tensile loads of about 456 N, Figure 6. According to this, the tensile stress in the area of the fracture reached 335 MPa, equating to 30 % of the initial wire tensile strength, Figure 6. The percentage elon-

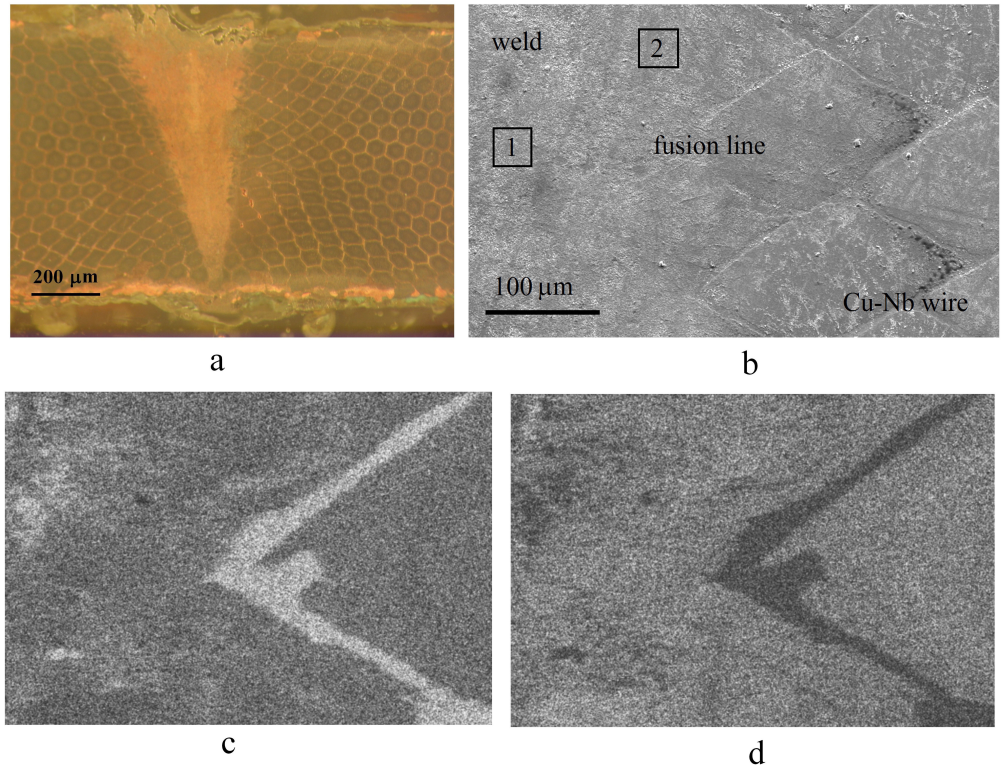


Figure 4. Structure of a joint welded without filler material: a) Penetration depth of laser after welding from one side; b) enlarged scanning electron microscope image of microstructure near the interface between the conductor and the weld; 1 and 2-denoted regions of energy-dispersive X-ray spectroscopy analysis; c) element map of copper in the weld area and fusion line; d) element map of niobium in the weld area and fusion line.

Bild 4. Struktur einer geschweißten Fuge ohne Zusatzwerkstoff: a) Eindringtiefe des Laserstrahls nach dem Schweißen von einer Seite; b) vergrößertes Rasterelektronenmikroskopbild des Gefüges nahe der Grenzfläche zwischen dem Leiter und der Schweißnaht; 1 und 2 bezeichnete Bereiche der energiedispersiven Röntgenspektroskopieanalyse; c) Elementkarte von Kupfer im Schweißbereich und in der Schmelzlinie; d) Elementkarte von Niobium im Schweißbereich und in der Schmelzlinie.

© 2019 WILEY-VCH Verlag GmbH & CO. KGaA, Weinheim

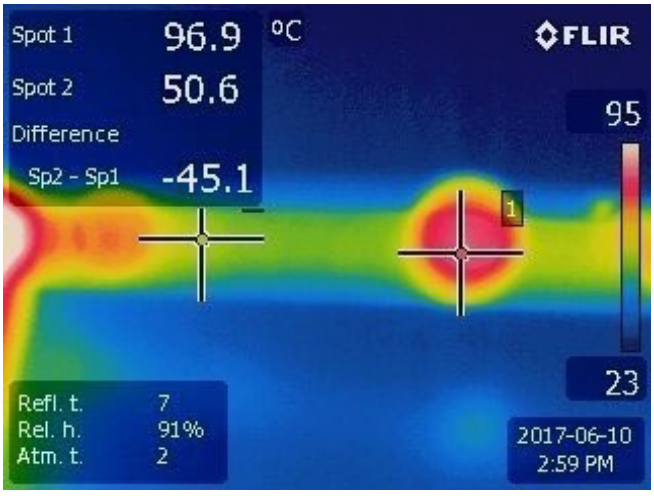


Figure 5. Distribution of temperature in the sample after 3 min of 60 A current flow: 1–measurement point in the joint area.

Bild 5. Temperaturverteilung in der Probe nach 3 min von 60 A Stromfluss: 1-Messpunkt im Fugenbereich.

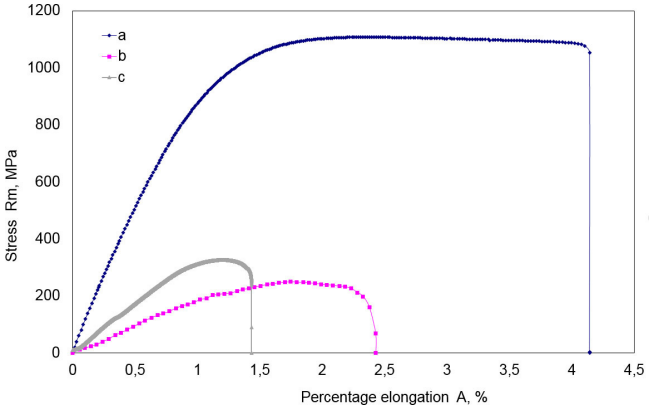


Figure 6. Stress-percentage elongation curves: a) Copper-niobium wire; b) sample with joint welded with a filler material; c) sample with joint welded without filler material; (break point-fusion area).

Bild 6. Dehnungskurven der Spannung – in Prozent: a) Kupfer-Niobium-Draht; b) Probe mit Fuge, die mit einem Füllmaterial verschweißt ist; c) Probe mit Fuge ohne Füllmaterial geschweißt; (Bruchstelle–Fusionsbereich).

gation of the sample of such connection after fracture was 1.5 %, which is about 35.7 % of the microcomposite wire percentage elongation.

According to the Kurnakov rule, the minimum tensile strength of copper−18 wt.% niobium weld could be about 237 MPa [53, 54]. The obtained tensile strength of the sample welded with filler material is slightly higher than this minimum value and the difference between measured and calculated minimal tensile strength of weld is about 5 %. The measured tensile strength of the sample welded without filler material joint is about 1.4 times higher than that calculated for the copper −18 wt.% niobium binary metal system, obtained after casting. However, autogenous laser welding joints have lower ductility than both initial microcomposite wire and laser welded joint obtained with the use of filler material.

9 Summary

On the basis of the above, it can be concluded that the tensile strength of a joint welded with filler material depends on applied filler material and is equal to the tensile strength of this material because all welded samples are broken through the weld area. The autogenous laser welding joints of copper-niobium microcomposite have higher tensile strength, which reaches 335 MPa, but such welded joints are very brittle due to very low ductility. From this point of view, a laser welding process applying more plastic filler material is reasonable. The microstructure of the autogenous weld consists mainly of a copper-based solid solution strengthened by niobium-rich precipitations. This structure of joint provides an insignificant increase in electrical resistance and sufficient ultimate strength. The weld obtained with use of filler material consists of two distinct zones. The outer one is formed mainly due to the melting of filler wire and consists of copper-based solid solution. The inside one consists of copper-based solid solution strengthened by niobium-rich precipitations. Such structure of the joint provides an insignificant increase in electrical resistance and sufficient ductility of the joint. The laser welding technology, in principle, is applicable for electric contact connections of the copper-niobium microcomposite wire. The laser welded joints are suitable for use in solenoid terminal connections with external electrical circuits that are not directly exposed to high magnetic or tensile forces that are generated inside a solenoid of a pulsed magnet system.

Acknowledgements

This work was supported, in part, under grant No. 09.3.3-LMT-K-712-06-0034 cofunded from the 2014-2020 Operational Programme for the European Union Funds Investments in Lithuania and

© 2019 WILEY-VCH Verlag GmbH & CO. KGaA, Weinheim

conducted by the Agency for Science, Innovation and Technology (MITA, Lithuania).

10 References

[1] F. Herlach, N. Miura, *High Magnetic Fields. Magnet Technology and Experimental Techniques.* Science and Technology, Volume 1, Imperial College Press London, **2003**.

[2] G.A. Shneerson, M.I. Dolotenko., S.I. Krivosheev, *Strong and Superstrong Pulsed Magnetic Fields Generation,* Studies in Mathematical Physics, De Gruyter, **2006**.

[3] K. Han, J.D. Embury, J.R. Sims, L.J. Campbell, H.J. Schneider-Muntau, V.I. Pantsyrnyi, A. Shikov, A. Nikitin, A. Vorobieva, *Mater. Sci. Eng.* **1999**, *267*, 99.

[4] L. Brandao, K. Han, J.D. Embury, R. Walsh, V. Toplosky, S. Van Sciver, *IEEE T. Appl. Supercon.* **2000**, *10*, 1282.

[5] L. Blumber, H. Hasizume, S. Ito, J. Minervini, N. Yanagi, *Fusion Sci. Technol.* **2011**, *60*, 635.

[6] H. Jones, M. Van Cleemput, A.L. Hickman, D.T. Ryan, P.M. Saleh, *Physica B.* **1998**, *246*, 337.

[7] D. Ciazynski, J. Duchateau, P. Decool, P. Libeyre, B. Turck, *Nucl. Fusion.* **2001**, *41*, 223.

[8] H.K. Yeo, K.H. Han, *J. Alloys Compd.* **2009**, *477*, 278.

[9] A.K. Shikov, V. Pantsyrnyi, A. Vorobeva, S. Sudev, N. Khlebova, A. Silajev, N. Belyakov, *Met. Sci. Heat Treat.* **2002**, *44*, 491.

[10] Y. Leprince-Wang, K. Han, Y. Huang, K. Yu-Zhang, *Mater. Sci. Eng.* **2003**, *A351*, 214.

[11] W. Głuchowski, J.P. Stobrawa, Z.M. Rdzawski, K. Marszowski, *J. Achiev. Mater. Manuf. Eng.* **2011**, *46*, 40.

[12] A. Jayanthi, K. Venkataramanan, K.S. Kumar, *IOSR J. Appl. Phys.* **2016**, *8*, 8.

[13] *Laser Welding Fundamentals.* Amada Miyachi America Inc, **2016**.

[14] Y.F. Tzeng, *Int. J. Adv. Manuf. Tech.* **2000**, *16*, 10.

[15] C. Walsh. *Laser Welding–Literature Review.* University of Cambridge, England, **2002**.

[16] D. Herrmann, P. Herzog, *Ind. Laser Solutions* **2013**, *1*, 14.

[17] B. Hitz, J.J. Ewing, J. Hetch, *Introduction to Laser Technology, 3rd Edition*, IEEE Press, New York, **2001**.

[18] S. Katayama, *Handbook of Laser Welding Technologies,* Technosfera, Moscow, **2015**.

[19] Y.N. Zhou, *Microjoining and Nanojoining*, Woodhead Publishing Limited, **2008**.

[20] A. Heider, R. Weber, D. Herrmann, P. Herzog, T. Graf, *J. Laser Appl.* **2015**, *27*, 022003.

[21] U. Reisgen, S. Olschok, C. Turner, *J. Laser Appl.* **2017**, *29*, 022402.

[22] M. Castillejo, P.M. Osii, L. Zhigilej, *Lasers in Materials Science. Chapter 1. Laser Physics for Materials Scientists*, Springer International Publishing, **2014**.

[23] M. Jokar, F.M. Ghaini, M.J. Torkamany, *J. Adv. Mater. Process.* **2013**, *1*, 35.

[24] E. Biro, D.C. Weckman, Y. Zhou, *Metall. Mater. Trans. A.* **2002**, *33 A*, 2019.

[25] B. Genc Oztoprak, E. Akman, M.M. Hanon, M. Gunes, S. Gumus, E. Kacar, O. Gundogdu, M. Zeren, A. Demir, *Opt. Laser Technol.* **2013**, *45*, 748.

[26] K. Hashimoto, T. Sato, K. Niwa, *J. Laser Appl.* **1991**, *3*, 21.

[27] G. Daurelio, G. Giorleo, *Mater. Manuf. Processes* **1991**, *6*, 577.

[28] H.C. Chen, G. Bi, M.L. Sharon Nai, J. Wei, *J. Mater. Process. Technol.* **2015**, *216*, 287.

[29] A. Heider, P. Stritt, A. Hess, R. Weber, T. Graf, *Phys. Procedia.* **2011**, *12*, 81

[30] A. Hess, R. Schuster, A. Heider, R. Weber, T. Graf, *Phys. Procedia.* **2011**, *12*, 88

[31] P. Bono, I. Metsios, J. Blackburn, P. Hilton, presented at *ICALEO 2013*, Miami, Florida, USA, October 6–10, **2013**, pp. 520.

[32] S.A.A. Akbari Mousavi, S.T. Niknejad, *J. Mater. Process. Technol.* **2010**, *210*, 1472.

[33] M. Banasik, J. Dworak, S. Stano, *Weld. Ind.* **2012**, *26*, 516.

[34] U. Dilthey, D. Fuest, W. Scheller, *Opt. Quantum Electron.* **1995**, *27*, 1181.

[35] Z. Sun, A.S. Salminen, *Mater. Manuf. Processes* **1997**, *12*, 759.

© 2019 WILEY-VCH Verlag GmbH & CO. KGaA, Weinheim

[36] A.G. Grigorjanc, *Fundamentals of Laser Treatment of Materials.* Mashinostrojenie, Moscow, **1989** (in Russian).
[37] Z. Sun, J.C. Ion, *J. Mater. Sci.* **1995**, *30*, 4205.
[38] A.G. Grigorjanc, I.N. Shiganov, A.I. Misiurov, *Technological Processes of Laser Treatment*, Moscow, Publishing House of Bauman Moscow State Technical University (BMSTU), Moscow, **2006**.
[39] S.I. Anisimov, Y.A. Imas, G.S. Romanov, Y.V. Khodyko, *The Effect of High-Power Laser Radiation on Metals,* Nauka, Moscow, **1970**.
[40] N. Višniakov, J. Novickij, D. Ščekaturovienė, A. Petrauskas, *Mater. Sci.-Medz.* **2011**, *17*, 16.
[41] M. M. Schwartz, *Brazing, 2nd Edition*, ASM International, Ohio, **2003**.
[42] N. Angelov, *Contemp. Mater.* **2015**, *6*, 62.
[43] V.P. Veiko, E.A. Shahno, *Laser Technology in Problems and Examples: textbook.* Publishing House of the University of Information Technologies, Mechanics and Optics,, ITMO", Saint Petersburg, **2014**.
[44] V.A. Parfenov, *Laser micromachnining of materials: textbook.* Publishing House of the Saint Petersburg Electrotechnical University,, ETU", Saint Petersburg, **2011**.
[45] W.M. Steen, J. Mazumder, *Laser Material Processing.* Springer-Verlag, London, **2010**.
[46] W.A. Ayoola, W.J. Suder, S.W. Williams, *J. Mater. Process. Technol.* **2017**, *249*, 522.
[47] X. Xue, A.B. Pereira, J. Amorim, J. Liao, *Metals.* **2017**, *7*, 292.
[48] S. Katayama, *Handbook of Laser Welding Technologies. Developments in Laser Microwelding Technology*, Woodhead Publishing Limited, **2013**.
[49] K.Y. Benyounis, A.G. Olabi, M.S.J. Hashmi, *J. Mater. Process. Technol.* **2005**, *164*, 978.
[50] *GOST 17441-84*, State Committee for Standardization, Moscow, **1984**.
[51] *GOST 10434-82*, State Committee for Standardization, Moscow, **1982**.
[52] S.P. Murzin, V.I. Artjushina, *Laser Equip. Technol.* **2006**, *2*, 441.
[53] N.S. Kurnakov, *Selected works. Volume 1*, Academy of Science USSR, Moscow, **1960**.
[54] N.S. Kurnakov, *Selected works. Volume 2*, Academy of Science USSR, Moscow, **1961**.

Received in final form: November 19th 2018

© 2019 WILEY-VCH Verlag GmbH & CO. KGaA, Weinheim